DALTON
FULL PAPER

Syntheses, crystal structures and (spectro)electrochemical studies of novel clusters $[Ru_4(\mu\text{-}H)_4(CO)_{10}(L)]$ [L = 2,2′-bipyrimidine, 2,3-bis(pyridin-2-yl)pyrazine, 2,2′-bipyridine] †

Jos Nijhoff,[a] Maarten J. Bakker,[a] František Hartl,*[,a] Gideon Freeman,[b] Scott L. Ingham[b] and Brian F. G. Johnson*[,c]

[a] *Anorganisch Chemisch Laboratorium, Institute of Molecular Chemistry, Universiteit van Amsterdam, Nieuwe Achtergracht 166, 1018 WV Amsterdam, The Netherlands*
[b] *Department of Chemistry, University of Edinburgh, West Mains Road, Edinburgh, UK EH9 3JJ*
[c] *University Chemical Laboratory, University of Cambridge, Lensfield Road, Cambridge, UK CB2 1EW*

Three tetrahedral clusters $[Ru_4(\mu\text{-}H)_4(CO)_{10}(L)]$ [L = 2,2′-bipyrimidine **1**, 2,3-bis(pyridin-2-yl)pyrazine **2** and 2,2′-bipyridine **3**] were obtained from a substitution reaction of $[Ru_4(\mu\text{-}H)_4(CO)_{12}]$ with L, involving the monosubstituted intermediates $[Ru_4(\mu\text{-}H)_4(CO)_{11}(\eta^1\text{-}L)]$. The solid-state structures of **1** and **3** have been elucidated by single-crystal X-ray analysis. In solution, dynamic behaviour of the hydride ligands in **1**–**3** was apparent from ^1H NMR spectra. UV/VIS and resonance-Raman spectroscopy established a significant $Ru(d_\pi)\rightarrow L(\pi^*)$ charge transfer (MLCT) character of the lowest electronic transition of **1**–**3** in the visible region. Consistent with the dominantly L(π*)-localized LUMO, one-electron reduction of **1** and **2** produced corresponding radical anions **1b** and **2b** which could be characterized by IR, UV/VIS and EPR spectroscopy. Subsequent one-electron reduction of **1b** and **2b** yielded unstable dianions $[Ru_4(\mu\text{-}H)_4(CO)_{10}(L)]^{2-}$ which were found to eliminate H_2. The dihydrido dianionic products **1c**, **2c** were also formed *via* slow disproportionation of **1b** and **2b**. The radical anion **3b**, containing the stronger σ-donor 2,2′-bipyridine anion, was detectable only on the subsecond time-scale of cyclic voltammetry. The electrochemically produced dihydrido dianion **3c** is similar but different from $[Ru_4(\mu\text{-}H)_2(CO)_{10}(bpy)]^{2-}$ **3c′** obtained by deprotonating **3** in reaction with NEt_4OH.

Tetranuclear hydridoruthenium carbonyl clusters have received considerable attention in homogeneous catalysis, in particular for their hydrogenation potential.[1] Promising research opportunities exist in the field of their selective photo- and electrochemical activation under substantially milder conditions of temperature and pressure. The particularly well known example is hydrogenation of ethylene photoinduced by $[Ru_4(\mu\text{-}H)_4(CO)_{12}]$ which proceeds without cluster fragmentation.[2] Elimination of hydrogen from the latter cluster also occurs on its electrochemical reduction. The intimate mechanism of this process has recently been reported by Osella *et al*.[3]

Another approach to redox activation of low-nuclearity transition-metal clusters involves co-ordination of redox active ligands. Their protecting role as electron reservoirs offers the possibility of (spectro)electrochemical characterization of otherwise short-lived reactive transients, in particular radicals, generated along the reduction path. This strategy has recently been applied for the clusters $[Os_3(CO)_{10}(\alpha\text{-diimine})]$. The introduction of the reducible α-diimine ligand permitted detailed investigation of the primary one-electron cathodic step followed by temperature-controlled splitting of an Os–Os(α-diimine) bond in $[Os_3(CO)_{10}(\alpha\text{-diimine})]^{\bullet -}$ and concomitant electron transfer producing a reactive open-structure dianionic species.[4]

In consequence of the aforementioned investigations, we became interested in the synthesis and electrochemistry of α-diimine-substituted derivatives of $[Ru_4(\mu\text{-}H)_4(CO)_{12}]$. This cluster is known[5,6] to undergo an efficient thermal substitution of carbonyl ligands by tertiary phosphines, producing $[Ru_4(\mu\text{-}H)_4(CO)_{12-n}(PR_3)_n]$ (n = 1–4), where n depends on the reaction conditions and the amount of phosphine added. A mixture of $[Ru_4(\mu\text{-}H)_4(CO)_{12-n}(PPh_3)_n]$ (n = 1–3) was also obtained under mild conditions *via* electrocatalytic (ETC) substitution reactions.[3]

In this paper we report on the targeted syntheses and characterization of the disubstituted derivatives $[Ru_4(\mu\text{-}H)_4(CO)_{10}(L)]$ [L = 2,2′-bipyrimidine (bpym), 2,3-bis(pyridin-2-yl)pyrazine (dpp) and 2,2′-bipyridine (bpy)], with bpy as the strongest σ-donor and bpym as the strongest π-acceptor in the series. Next, we have performed a (spectro)electrochemical study of their redox properties and reduction paths, aimed at comparison with the unsubstituted precursor $[Ru_4(\mu\text{-}H)_4(CO)_{12}]$ and with the related clusters $[Os_3(CO)_{10}(\alpha\text{-diimine})]$. The ligands L and the adopted numbering schemes are shown in Fig. 1.

Experimental

Materials

The cluster $[Ru_4(\mu\text{-}H)_4(CO)_{12}]$ was synthesized from $[Ru_3(CO)_{12}]$ in a magnetically stirred Burghoff (250 ml) autoclave according to the literature method.[7] 2,2′-Bipyrimidine (Alfa and Lancaster Chemicals), 2,3-bis(pyridin-2-yl)pyrazine and 2,2′-bipyridine (both Aldrich) were used as purchased. Trimethylamine *N*-oxide dihydrate, $Me_3NO{\cdot}2H_2O$ (Alfa), was carefully dried by first refluxing the sample (15 g) in benzene (250 ml), typically overnight, to remove the water of crystallisation *via* Dean–Stark distillation. The benzene was then decanted off

† *Supplementary data available*: interpretation of the ^1H NMR decoupling experiments carried out on complex **2** to assign the proton resonances of the dpp ligand: off resonance irradiation at δ 11.00, and irradiation at δ 8.89, 8.67 and 7.34. For direct electronic access see http://www.rsc.org/suppdata/dt/1998/2625/, otherwise available from BLDSC (No. SUP 57401, 5 pp.) or the RSC Library. See Instructions for Authors, 1998, Issue 1 (http://www.rsc.org/dalton).
Non-SI unit employed: G = 10^{-4} T.

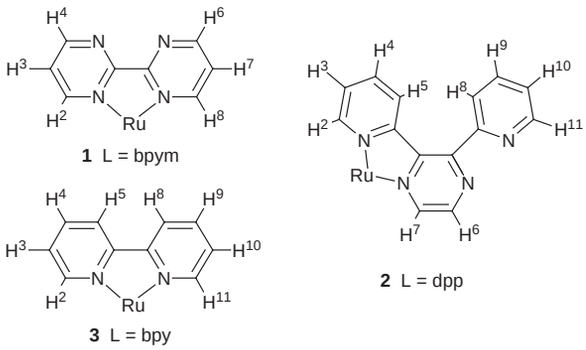

Fig. 1 Structures of the ligands L and adopted numbering schemes for clusters **1**–**3**

and the sample dried under vacuum on a Schlenk line, and sublimed prior to use. The supporting electrolyte NBu_4PF_6 (Aldrich) was dried *in vacuo* at 80 °C for 10 h. The salt NEt_4OH was purchased from Fluka as a 25% solution in MeOH. Ferrocene (Fc) was used as received from BDH. Solvents (all Acros Chimica, analytical grade) were dried using a benzophenone–sodium mixture (THF, benzene), sodium wire (hexane), P_2O_5 (CH_2Cl_2) or CaH_2 (MeCN), and freshly distilled under nitrogen. Silica gel (Kieselgel 60, Merck, 70–230 mesh) for column chromatography was dried and activated by heating overnight *in vacuo* at 160 °C. Preparative TLC was carried out using glass plates (20 × 20 cm) supplied by Merck, coated with a 0.25 cm layer of Kieselgel 60 F_{254}.

Syntheses of $[Ru_4(\mu\text{-}H)_4(CO)_{10}(L)]$ (L = bpym 1, dpp 2 or bpy 3)

All clusters **1**–**3** were prepared according to the following general procedure. A solution of 200 mg $[Ru_4(\mu\text{-}H)_4(CO)_{12}]$ and 2.5 equivalents of L (L = bpym, dpp or bpy) in dichloromethane (150 ml) was cooled to 195 K in a dry ice–acetone bath. The reaction was initiated by the dropwise addition of 2.2 equivalents of Me_3NO in dichloromethane (20 ml) over a 20 min period under stirring. After stirring for an additional 10 min the mixture was allowed to warm gradually to room temperature and was observed to change colour from yellow-orange to green (for L = bpym or bpy) and finally to deep red-brown. The solvent was evaporated and the crude product was separated from unreacted $[Ru_4(\mu\text{-}H)_4(CO)_{12}]$ by using either TLC with hexane–dichloromethane (3 : 7 v/v, for L = bpy or dpp) or 100% dichloromethane (for L = bpym) as eluent, or by column chromatography by gradual elution with hexane–dichloromethane mixtures (initially 1 : 9 v/v). All preparations and purifications were performed under a nitrogen atmosphere using Schlenk techniques. The purity of the cluster **1**–**3** was checked with elemental analysis or mass spectroscopy. All compounds were characterized by IR, ^{1}H NMR (see Fig. 1 for the adopted numbering schemes) and UV/VIS spectroscopy.

$[Ru_4(\mu\text{-}H)_4(CO)_{10}(bpym)]$ 1. IR [ν(CO)/cm^{-1}; THF]: 2073m, 2042s, 2018s, 2000m, 1979m, 1945w. ^{1}H NMR ($CDCl_3$): δ 9.16 (dd, J = 2.17, 4.74, 2 H, H^2, H^8), 9.07 (dd, J = 2.15, 5.66, 2 H, H^4, H^6), 7.62 (dd, J = 4.80, 5.61 Hz, 2 H, H^3, H^7), −15.9 (s, 2 H), −21.5 (s, 2 H). UV/VIS [λ_{max}/nm (ε_{max}/M^{-1} cm^{-1}); CH_2Cl_2]: 495 (3350), 359 (13 700) [Found (calc. for $C_{18}H_{10}N_4O_{10}Ru_4$): C, 25.68 (25.66); H, 1.37 (1.20); N, 6.18 (6.65%)].

$[Ru_4(\mu\text{-}H)_4(CO)_{10}(dpp)]$ 2. IR [ν(CO)/cm^{-1}; THF]: 2073m, 2041s, 2018vs, 2000m, 1979m, 1946w. ^{1}H NMR ($CDCl_3$): δ 8.92 (d, J = 2.96, 1 H, H^7), 8.89 (d, 1 H, H^2), 8.67 (d, J = 2.9, 2 H, H^6, H^{11}), 8.04 (td, J = 1.75, 7.71, 1 H, H^9), 7.94 (ddd, J = 1.11, 1.21, 7.90, 1 H, H^8), 7.56 (m, 2 H, H^4, H^{10}), 7.34 (ddd, J = 1.45, 5.45, 7.62, 1 H, H^3), 7.04 (d, J = 8.37 Hz, 1 H, H^5), −15.8 (vw, br), −21.3 (w br). UV/VIS [λ_{max}/nm (ε_{max}/M^{-1} cm^{-1}); CH_2Cl_2]: 513 (3640), 357 (15 500) and 276 (26 700). Mass (FAB$^+$): (m/z)$^+$ 925 (922 calc.) [M]$^+$ [Found (calc. for $C_{24}H_{14}N_4O_{10}Ru_4$): C, 31.12 (31.24); H, 1.62 (1.53); N, 5.91 (6.07%)].

$[Ru_4(\mu\text{-}H)_4(CO)_{10}(bpy)]$ 3. IR [ν(CO)/cm^{-1}; THF]: 2071m, 2039vs, 2015vs, 1996s, 1974m, 1947sh. ^{1}H NMR ($CDCl_3$): δ 8.92 (d, J = 5.78, 2 H, H^2, H^{11}), 8.11 (d, J = 6.6, 2 H, H^5, H^8), 7.96 (dt, J = 7.52 and 1.55, 2 H, H^4, H^9), 7.44 (ddd, J = 7.49, 5.61, 1.49 Hz, H^3, H^{10}), −15.68 (s, 2 H), −21.45 (s, 2 H). UV/VIS [λ_{max}/nm (ε_{max}/M^{-1} cm^{-1}); CH_2Cl_2]: 476 (3210), 357 (12 100) and 301 (32 600). Mass (FAB$^+$): (m/z)$^+$ 845 (844 calc.) [M]$^+$ [Found (calc. for $C_{20}H_{12}N_2O_{10}Ru_4$): C, 28.27 (28.44); H, 1.49 (1.43); N, 3.14 (3.32%)].

Attempted synthesis of $[Ru_4(\mu\text{-}H)_4(CO)_8(bpym)_2]$

A solution of 155 mg $[Ru_4(\mu\text{-}H)_4(CO)_{12}]$ in 150 ml CH_2Cl_2 was cooled to −78 °C before addition of 2,2′-bipyrimidine (91 mg, 2.8 equivalents, dissolved in 10 ml CH_2Cl_2). Trimethylamine *N*-oxide (66 mg, 4.2 equivalents, in 25 ml CH_2Cl_2) was then added dropwise to the reaction mixture over a 20 min period. The solution turned from dark green to deep red on gradual warming to room temperature. A large amount of unassigned insoluble material was formed in addition to a red product which was purified by TLC (100% CH_2Cl_2 as eluent) and identified by IR and mass spectroscopy as **1** and not $[Ru_4(\mu\text{-}H)_4(CO)_8(bpym)_2]$.

X-Ray crystallography

Crystals of the clusters **1** and **3** suitable for single-crystal X-ray analysis were grown from a dichloromethane–hexane solution at −20 °C (**1**) or 5 °C (**3**). Despite repeated attempts crystals of **2** have not been obtained. Data collection was performed on a Stoë Stadi four-circle diffractometer, equipped with an Oxford Cryosystems low-temperature device. The intensities were reduced to F_o^2 and an empirical absorption correction based on semiempirical ψ-scan data was applied. The structures were solved by direct methods, followed by Fourier-difference and full-matrix least-squares refinements on F^2 using the computer programs SHELXS 86 and SHELXL 93 and Figs. 2 and 3 generated using ORTEP.[8]

Crystal data for $[Ru_4(\mu\text{-}H)_4(CO)_{10}(bpym)]$ 1. $C_{18}H_{10}N_4O_{10}Ru_4\cdot CH_2Cl_2$, M = 929.49, monoclinic, a = 8.474(2), b = 18.897(4), c = 18.400(5) Å, β = 92.15(2)°, U = 2944.4(1) Å^3, T = 150(2) K, space group $P2_1/c$, Z = 4, μ(Mo-Kα) = 2.248 mm^{-1}, 4549 reflections collected, 3842 reflections independent (R_{int} = 0.0208) which were used in all calculations. The final $wR(F^2)$ was 0.1024; $R1$ = 0.0431.

Crystal data for $[Ru_4(\mu\text{-}H)_4(CO)_{10}(bpy)]$ 3. $C_{20}H_{12}N_2O_{10}Ru_4\cdot 0.25\ CH_2Cl_2$, M = 865.83, triclinic, a = 8.6204(10), b = 9.9099(12), c = 16.431(2) Å, α = 73.625(10), β = 84.345(10), γ = 88.371(9)°, U = 1340.1(3) Å^3, T = 293(2) K, space group $P\bar{1}$, Z = 2, μ(Mo-Kα) = 2.314 mm^{-1}, 4728 reflections collected, 4728 reflections independent which were used in all calculations. The final $wR(F^2)$ was 0.0994; $R1$ = 0.0347.

CCDC reference number 186/1056.

Spectroscopic measurements

The UV/VIS absorption spectra were recorded on software-updated Perkin-Elmer Lambda 5 or Varian Cary 4E spectrophotometers, FTIR spectra on Bio-Rad FTS-7 or Perkin-Elmer 1600 spectrometers, and ^{1}H NMR spectra on Bruker WH 250 MHz or AMX 300 spectrometers. X-Band EPR spectra were recorded on a Varian Century E-104A spectrometer. 2,2′-Diphenyl-1-picrylhydrazyl (DPPH) was employed as an external '*g* mark'. Mass spectra (FAB$^+$) were measured on a Kratos MS50TC spectrometer, calibrated with CsI. The

samples were run in a matrix solution (*m*-nitrobenzyl alcohol, 3-NOBA). Resonance-Raman measurements were performed using a Dilor Modular XY spectrometer which employs a back-scattering geometry and a multichannel diode array detection system. Spectra were taken from KNO_3 pellets at room temperature. Excitation lines of wavelengths 457.9, 476.5, 496.5 and 514.4 nm were obtained from an SP model 2016 Ar^+ laser.

(Spectro)electrochemical measurements

Cyclic voltammograms were recorded in a gastight cell under a nitrogen atmosphere. The cell was equipped with Pt disc working (apparent surface area of 0.42 mm^2), Pt gauze auxiliary, and Ag wire pseudo-reference electrodes. The working electrode was carefully polished with a 0.25 μm grain diamond paste. The scan rate was varied between 0.02 and 2 V s^{-1}. All redox potentials are reported against the ferrocene–ferrocenium (Fc/Fc^+) redox couple used as an internal standard[9] [$E_{\frac{1}{2}}(Fc/Fc^+)$ = +0.58 V *vs*. SCE in THF]. The solutions for cyclic voltammetric experiments were typically 2×10^{-3} M in the cluster compounds and 3×10^{-1} M in NBu_4PF_6. The potential control was achieved with a PAR model 283 potentiostat equipped with positive feedback for ohmic-drop compensation. Bulk electrolyses were carried out in a gastight cell that consisted of three chambers separated at the bottom by S4 frits, with a Pt-flag working electrode (120 mm^2 surface) in the middle, and Ag wire pseudo-reference and Pt gauze auxiliary electrodes in the lateral chambers. The concentrations used were 5×10^{-3} M **1** and **2** and 3×10^{-1} M NBu_4PF_6. Infrared and UV/VIS spectroelectrochemical experiments at room temperature were performed with an optically transparent thin layer electrode (OTTLE) cell,[10] equipped with a Pt minigrid working electrode (32 wires per cm) and CaF_2 optical windows. For IR and UV/VIS spectroelectrochemistry at low temperatures another OTTLE cell[11] was employed which fitted into a liquid-nitrogen cryostat.[12] The spectroelectrochemical samples were typically 10^{-2} M in the cluster compounds. A PA4 potentiostat (EKOM, Czech Republic) was used to carry out the controlled-potential electrolyses.

Results and Discussion

Syntheses of $[Ru_4(\mu\text{-}H)_4(CO)_{10}(L)]$

In contrast to the availability of $[Ru_4(\mu\text{-}H)_4(CO)_{12-n}(PR_3)_n]$ (n = 1–4),[5,6] the substitution reaction of $[Ru_4(\mu\text{-}H)_4(CO)_{12}]$ with an excess of the α-diimine ligand (L), initiated by an addition of 2.2 equivalents of Me_3NO, resulted in the overall substitution of two carbonyl ligands, producing stable $[Ru_4(\mu\text{-}H)_4(CO)_{10}(L)]$ (L = bpym **1**, dpp **2**, bpy **3**) in 10–20% yield. Attempts to synthesize the tetrasubstituted clusters $[Ru_4(\mu\text{-}H)_4(CO)_8(L)_2]$ using 4.2 equivalents of Me_3NO were unsuccessful. A similar situation applies for related $[Os_3(CO)_{12}]$ which only affords the disubstituted cluster $[Os_3(CO)_{10}(L)]$.[4,13]

Irrespective of whether the reaction of $[Ru_4(\mu\text{-}H)_4(CO)_{12}]$ with L was carried out using 1.1 or 2.2 equivalents of Me_3NO, only two carbonyl ligands were removed and substituted by the α-diimine. Addition of 2.2 equivalents of Me_3NO only increased the yield of $[Ru_4(\mu\text{-}H)_4(CO)_{10}(L)]$. For L = bpy or bpym, however, a green intermediate was observed during the reaction course at low temperatures. For L = bpym, this species was stable enough at $T \leqslant 195$ K to permit recording of its IR spectrum which showed ν(CO) bands at 2080m, 2066s, 2053s, 2029m, 2022m and 2005w cm^{-1} (in CH_2Cl_2). The spectrum is virtually identical to that of $[Ru_4(\mu\text{-}H)_4(CO)_{11}(py)]$ [ν(CO) at 2087vw (sh), 2080m, 2066s, 2056m, 2029m, 2022m (sh), 2006w, 1989vw (br) cm^{-1}][14] and closely resembles that of $[Ru_4(\mu\text{-}H)_4(CO)_{11}\{P(OMe)_3\}]$.[15] The green intermediate is therefore most likely the monosubstituted cluster $[Ru_4(\mu\text{-}H)_4(CO)_{11}(\eta^1\text{-}L)]$ where L co-ordinates in a monodentate fashion. We therefore conclude that the formation of $[Ru_4(\mu\text{-}H)_4(CO)_{10}(L)]$ is a stepwise process, as depicted in Scheme 1. It is probably the chelate effect which favours this substitution pattern. The CO-extrusion reaction of the η^1-bound α-diimine was discussed in detail by Lees and co-workers for $[M(CO)_n(\alpha\text{-diimine})]$ (n = 4 or 5; M = Cr, Mo or W).[16]

Table 1 Selected bond lengths (Å) and angles (°) for $[Ru_4(\mu\text{-}H)_4(CO)_{10}(bpym)]$ **1**

Ru(1)–Ru(2)	2.944(12)	Ru(2)–H(2)	1.74(3)
Ru(1)–Ru(3)	2.787(13)	Ru(2)–H(3)	1.75(3)
Ru(1)–Ru(4)	2.760(11)	Ru(3)–H(3)	1.75(3)
Ru(2)–Ru(3)	3.035(12)	Ru(3)–H(4)	1.75(3)
Ru(2)–Ru(4)	2.949(13)	Ru(4)–H(2)	1.75(3)
Ru(3)–Ru(4)	2.931(12)	Ru(4)–H(4)	1.74(3)
Ru(2)–C(21)	1.834(11)	mean Ru–C	1.89
Ru(2)–N(1b)	2.099(8)	mean C–O	1.13
Ru(2)–N(4b)	2.117(8)	N(1b)–Ru(3)–N(4b)	77.4(3)
Ru(2)–H(1)	1.74(3)		

Table 2 Selected bond lengths (Å) and angles (°) for $[Ru_4(\mu\text{-}H)_4(CO)_{10}(bpy)]$ **3**

Ru(1)–Ru(2)	2.925(7)	Ru(1)–H(4)	1.76(3)
Ru(1)–Ru(3)	3.023(7)	Ru(2)–H(2)	1.77(3)
Ru(1)–Ru(4)	2.795(8)	Ru(2)–H(4)	1.77(3)
Ru(2)–Ru(3)	2.964(7)	Ru(3)–H(1)	1.76(3)
Ru(2)–Ru(4)	2.780(8)	Ru(3)–H(2)	1.75(3)
Ru(3)–Ru(4)	2.946(7)	Ru(3)–H(3)	1.76(3)
Ru(3)–C(31)	1.844(7)	Ru(4)–H(3)	1.76(3)
Ru(3)–N(1)	2.095(5)	mean Ru–C	1.90
Ru(3)–N(2)	2.090(5)	mean C–O	1.13
Ru(1)–H(1)	1.76(3)	N(1)–Ru(3)–N(2)	77.4(2)

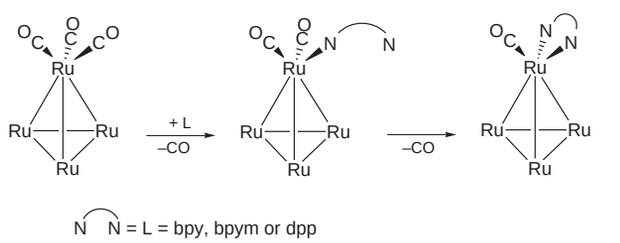

Scheme 1 Stepwise formation of the disubstituted clusters $[Ru_4(\mu\text{-}H)_4(CO)_{10}(L)]$

Solid-state structure of $[Ru_4(\mu\text{-}H)_4(CO)_{10}(L)]$ (L = bpym 1 or bpy 3)

The isotropic solid-state structures of **1** and **3** are depicted in Fig. 2A and 2B, respectively. Selected bond lengths and angles of **1** and **3** are listed in Tables 1 and 2, respectively.

The crystal structures of **1** and **3** confirm that the α-diimine ligand is bound in a bidentate fashion through the nitrogen lone pairs to a single ruthenium atom bearing only one terminal CO group. All ten carbonyl ligands are terminal, as could also be inferred from the IR spectra (see below). The bite angle N–Ru–N is 77.4° for both **1** and **3**. Notably, the Ru–N bond lengths of 2.099(8) and 2.117(8) Å in **1** are considerably longer than those in **3** [2.095(5) and 2.090(5) Å]. This difference reflects the electron-withdrawing character of the unco-ordinated nitrogen atoms of the 2,2′-bipyrimidine ligand, responsible for reduced N→Ru σ-donation which results in weaker Ru–N bonds in **1**. The apical bonds Ru(2)–C(21) in **1** and Ru(3)–C(31) in **3** are shorter than the other Ru–CO bonds in these clusters due to the increased electron density and hence stronger Ru→CO π-back bonding at the α-diimine-substituted site. The Ru_4 core is edge-bridged by four hydride ligands, three of them spanning the Ru–Ru (L) bonds. The hydride positions, localized from Fourier-difference maps of the low-angle diffraction data, are also indicated by distortion of the tetrahedral cluster geometry due to lengthening of the four hydride-

Table 3 Raman wavenumbers of co-ordinated 2,2′-bipyrimidine from resonance-Raman spectra of $[Ru_4(\mu\text{-}H)_4(CO)_{10}(bpym)]$ **1** in KNO_3 at room temperature, compared with those of related complexes $[W(CO)_4(bpym)]$[19] and $[Os_3(CO)_{10}(bpym)]$[13]

Compound	ν/cm^{-1}						
1	1575	1548	1466	1415	1335	1203	1025
$[W(CO)_4(bpym)]$	1577	1548	1463	1417	1335	1198	1017
$[Os_3(CO)_{10}(bpym)]$	1578	1537	1463	1407	1340	1194	1018

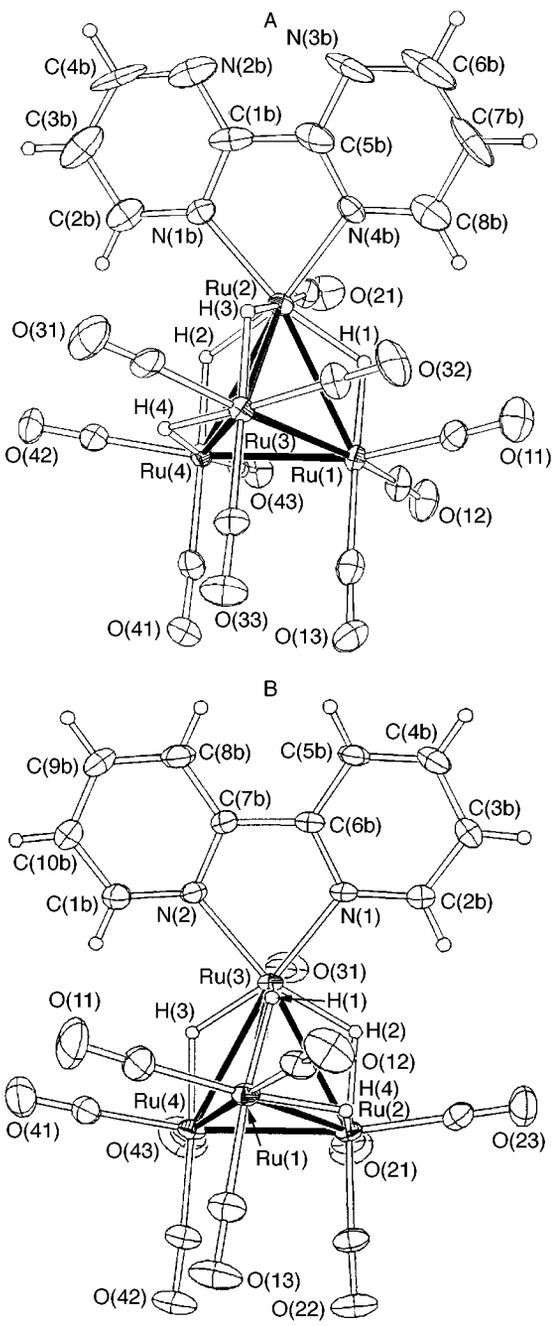

Fig. 2 A, An ORTEP drawing of the crystal structure of $[Ru_4(\mu\text{-}H)_4(CO)_{10}(bpym)]$ **1**. B, An ORTEP drawing of the crystal structure of $[Ru_4(\mu\text{-}H)_4(CO)_{10}(bpy)]$ **3**

bridged Ru–Ru bonds [average Ru–Ru distance 2.964(6) Å in **1** and 2.964(5) Å in **3**] compared to the two unbridged Ru–Ru bonds [average Ru–Ru distance 2.773(4) Å in **1** and 2.787(4) Å in **3**]. Similar deformation of the metal core has been reported for other tetrahedral Ru_4 clusters with bridging hydride ligand(s).[6,17]

Spectroscopic properties of $[Ru_4(\mu\text{-}H)_4(CO)_{10}(L)]$

IR and ^{1}H NMR spectroscopy. The infrared spectra of **1**–**3** in the CO stretching region are very similar and correspond to terminal co-ordination of all carbonyl ligands. The slightly larger ν(CO) wavenumbers of **1** and **2** relative to those of **3** reflect less pronounced Ru→CO π-back donation due to the larger π-acceptor capacity of the bpym and dpp ligands compared to that of the bpy ligand.[18]

The ^{1}H NMR data of **1** and **3** (see Experimental section) confirm that the bpy and bpym ligands co-ordinate to Ru in a normal bidentate fashion. The two aromatic rings of these ligands remain magnetically equivalent upon co-ordination. For cluster **1**, the D_{2h} symmetry of the free bpym ligand is lost upon co-ordination. The ^{1}H NMR resonances of the cluster **2** could be completely assigned with the aid of decoupling experiments described in detail in SUP 57401. The chemical shift of the *ortho* protons adjacent to the co-ordinated nitrogen atoms to lower values by 0.12–0.50 ppm in comparison with the resonances of the unco-ordinated ligands L is characteristic for σN, σN′-co-ordination of L to a low-valent metal centre. This effect arises from a larger contribution of a resonance form in which the nitrogen atoms bear a partial negative charge and the adjacent carbon atoms a corresponding partial positive charge.

Notably, the hydride resonances show a higher symmetry than expected from the solid-state structures. There are two hydride resonances around δ −16 and −22, each accounting for two protons. The signals are rather weak and broad, indicating that a fluxional process may well be responsible for their pairwise equivalence.

Electronic absorption and resonance-Raman spectra. The clusters **1**–**3** are orange to red-brown in colour. Their UV/VIS absorption maxima and corresponding molar absorption coefficients in CH_2Cl_2 are listed in the Experimental section. The position of the lowest energy absorption band depends on the electronic properties of the α-diimine ligands L and on the solvent polarity. For **3**, the absorption maximum shifts from 486 nm in benzene to 463 nm in THF and 447 nm in acetonitrile. In contrast to this, the absorption maxima at higher energy hardly show any solvatochromism. The negative solvatochromism and the low-energy shift of λ_{max}, resulting from replacement of 2,2′-bipyridine by the stronger π-acceptor 2,2′-bipyrimidine (from 463 to 484 nm in THF) point to a charge-transfer character of the lowest-energy electronic transition. Its nature was further investigated by resonance-Raman (rR) spectroscopy on visible excitation of **1** with four different Ar^+ laser lines (see Experimental section). The result is presented in Table 3.

The main rR effect is observed for bands in the 1000–1600 cm^{-1} region which belong to internal stretching modes of the 2,2′-bipyrimidine ligand. The presence of the Raman band at 1335 cm^{-1}, which is assigned to the inter-ring C–C stretching vibrations, indicates population of the lowest $\pi^*(b_{2u})$ orbital of 2,2′-bipyrimidine in the charge-transfer excited state.[19] Importantly, the peak due to the resonance enhanced ν_s(CO) vibration of **1** also showed up at 2070 cm^{-1}, indicating depopulation of the Ru(d_π) orbitals involved in the Ru→CO π-back bonding. The combined resonance-Raman and UV/VIS features thus reveal that the lowest electronic transition of $[Ru_4(\mu\text{-}H)_4(CO)_{10}(L)]$ is directed towards the α-diimine ligand L, having a significant Ru(d_π)→L(π^*) charge-transfer (MLCT) character.

(Spectro)electrochemical studies of $[Ru_4(\mu\text{-}H)_4(CO)_{10}(L)]$

The redox properties of clusters **1**–**3** and their reduction paths were investigated by cyclic voltammetry, IR and UV/VIS spectroelectrochemistry, and by EPR spectroscopy. Redox potentials of **1**–**3** and their reduction products are presented in Table 4. Cyclic voltammograms of **2** and **3** are depicted in Fig. 3. Infrared ν(CO) wavenumbers and UV/VIS spectroscopic

Table 4 Redox potentials of the clusters **1**–**3** and their reduction products[a]

Cluster	E_{pc} (R_1)[b]	ΔE_p (R_1/O_1)	E_{pc} (R_2)[c]	E_{pc} (R_3)[d]	E_{pa} (O_m)[e]	E_{pa} (O_2')[f]
1	−1.54	0.12	−2.23	−2.38	+0.39	−1.04
2	−1.57	0.11	−2.23	−2.38	+0.41	−1.08
3	−1.88	0.14	−2.35	−2.42	+0.35	−1.17

[a] Conditions: 2×10^{-3} M **1**–**3** in THF–3×10^{-1} M NBu_4PF_6, $T = 298$ K, Pt disc electrode, $\nu = 100$ mV s^{-1}; potentials given in V *vs.* $E_{\frac{1}{2}}(Fc/Fc^+)$ (= +0.575 V *vs.* SCE); $\Delta E_p(Fc/Fc^+) = 0.11$ V. [b] Reduction (1e) of **1**–**3**. [c] Reduction (1e) of the corresponding radical anions **1b**–**3b**. [d] Reduction (1e) of the dihydrido dianions **1c**–**3c**. [e] Oxidation of **1**–**3**. [f] Oxidation of the dihydrido dianions **1c**–**3c**.

Table 5 IR ν(CO) wavenumbers of the clusters **1**–**3** and their electrochemical reduction products

	ν/cm^{-1}					
1[a,b]	2073m	2042s	2018s	2000m	1979w	1945w
1b[a,b]	2065m	2033s	2008s	1989m	1970w	1943w
1c[b]	2006w	1979m	1956 (sh)	1929s (br)	1889s	1867 (sh)
	1770 (sh)	1736m/w	1712w	1677vw		
2[a,b]	2073m	2041s	2018s	2000m	1979m	1946w
2[c]	2074m	2042s	2017s	1999m	1979m	1942w
2b[a,b]	2063m	2031s	2006s	1986m	1966w	1942w
2b[c]	2066m	2033s	2008s	1987m	1966w	1941w
2c[b]	2008m	1979m	1957s	1934s (br)	1892s	1875 (sh)
	1762 (sh)	1744m	1724m/w	1678vw		
3[b]	2071m	2039vs	2015vs	1996s	1974m	1947 (sh)
3c[b]	2025w	1990s	1956 (sh)	1948vs	1923s	1910 (sh)
	1879m	1862 (sh)	1771 (sh)	1735w	1712w	1670vw
3e[b]	1985vw	1948m	1905s	1892s	1848m	1831m
	1707w	1680w				

[a] In CH_2Cl_2–electrolyte at $T = 298$ K. [b] In THF–electrolyte at $T = 298$ K. [c] In CH_2Cl_2–electrolyte at $T = 223$ K.

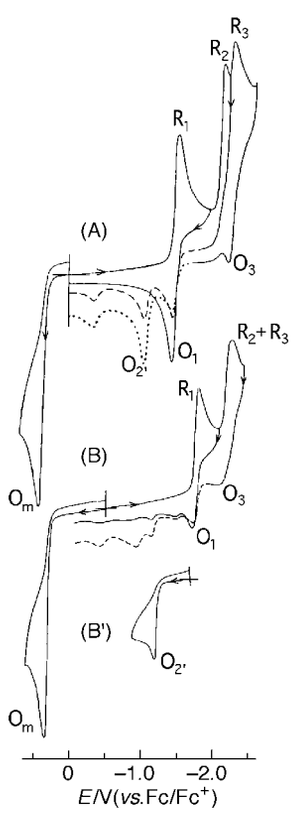

Fig. 3 Cyclic voltammograms of **2** (A) and **3** (B). Oxidation of **3c** generated *via* bulk electrolysis of **3** at $E(R_1)$ (B^1). Conditions: Pt disc microelectrode (0.42 mm^2 apparent surface), THF–NBu_4PF_6, $T = 298$ K, $\nu = 0.1$ V s^{-1}

data of **1**–**3** and their reduction products are collected in Tables 5 and 6, respectively.

Radical anions $[Ru_4(\mu\text{-}H)_4(CO)_{10}(L)]^{\bullet -}$ (L = bpym or dpp). Reduction of the clusters **1** and **2** [cathodic peak R_1 in Fig. 3(A)] is both electrochemically and chemically reversible on the subsecond time-scale of cyclic voltammetry (defined by $\nu \geqslant 0.02$ V s^{-1}), satisfying the usual diagnostic tests.[20] The product of this cathodic step was further studied *in situ* by IR and UV/VIS spectroelectrochemistry in a thin-layer cell. Fig. 4 shows the IR/UV/VIS spectral changes accompanying the reduction of **1**. The ν(CO) pattern of **1** remains preserved on reduction, being shifted by some 9–12 cm^{-1} to smaller wavenumbers. The retention of isosbestic points indicates stability of the reduction product at room temperature over a period of *ca.* 10 min. After this period, however, a slow secondary reaction was evident from gradually increasing absorbances below 1900 cm^{-1}. This secondary reaction was not observed at $T \leqslant 253$ K, allowing characterization of the primary reduction product, denoted as **1b**, by UV/VIS spectroscopy [see Fig. 4(a)]. The most prominent features of the UV/VIS spectrum of **1b** are the two sharp absorption bands at 475 and 503 nm, accompanied by a lower-lying broad absorption band with $\lambda_{max} \approx 850$ nm. These bands can straightforwardly be attributed to intra-ligand (IL) electronic transitions of the co-ordinated radical anion $[bpym]^{\bullet -}$.[19,21] From the cyclic voltammetric and spectro-electrochemical experiments it is concluded that the reduction of **1** is a one-electron process which produces the corresponding radical anion $[Ru_4(\mu\text{-}H)_4(CO)_{10}(bpym)]^{\bullet -}$ **1b** with the odd electron dominantly localized on the lowest π* orbital of the 2,2′-bipyrimidine ligand. This also applies for **2**. In this case, however, the radical anion **2b** (see Tables 5 and 6) partly decomposed in CH_2Cl_2 at room temperature in the course of the reduction of **2**, *i.e.* more rapidly than **1b** under the same conditions. The decomposition significantly slowed down in less polar THF. The UV/VIS spectra of **2b** (see Table 6) were recorded in CH_2Cl_2 at $T = 223$ K where the radical anion remained inherently stable and could be fully reoxidized back to **2**.

The radical nature of **1b** and **2b** was unambiguously confirmed by recording their EPR spectra (see Fig. 5). For this purpose **1b** and **2b** were generated in THF at $T = 263$ K by bulk electrolysis at the cathodic potential $E(R_1)$. The EPR spectra, found at $g = 2.0015$ for **1b** and $g = 2.0016$ for **2b** (*i.e.* close to the

Table 6 UV/VIS spectra of the clusters **1**–**3** and some of their reduction products

	λ_{max}/nm (ε_{max}/M^{-1} cm^{-1})				
1[a]	256 (sh) (31 000)	358 (13 700)	484 (3350)		
1b[a]	278 (sh) (23 000)	362 (20 200)	475 (7000)	503 (7150)	850 (650)
2[b]	274 (41 500)	357 (15 500)	486 (3700)		
2b[b]	266 (sh) (39 000)	349 (23 500)	459 (sh) (9000)		830 (1450)
3[c]	301 (32 600)	354 (12 100)	463 (3200)		
3c[c]	336 (12 600)		*ca.* 500 (sh)	763 (1500)	

[a] In CH_2Cl_2 at $T = 253$ K. [b] In CH_2Cl_2 at $T = 223$ K. [c] In THF at $T = 298$ K. All solutions contained 3×10^{-1} M NBu_4PF_6.

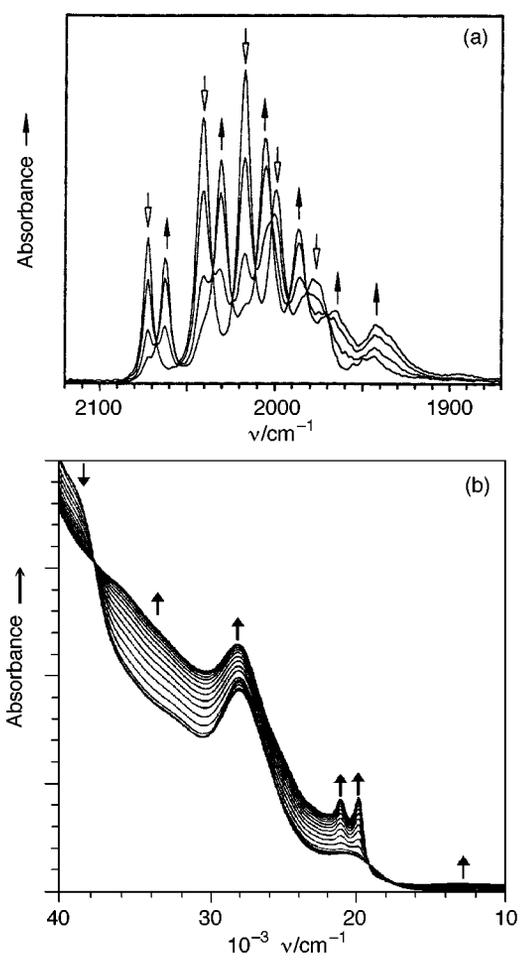

Fig. 4 Spectral changes in the IR ν(CO) [(a), in THF at $T = 298$ K] and UV/VIS [(b), in CH_2Cl_2 at $T = 253$ K] regions, accompanying the reversible reduction of the cluster **1** producing the radical anion **1b**

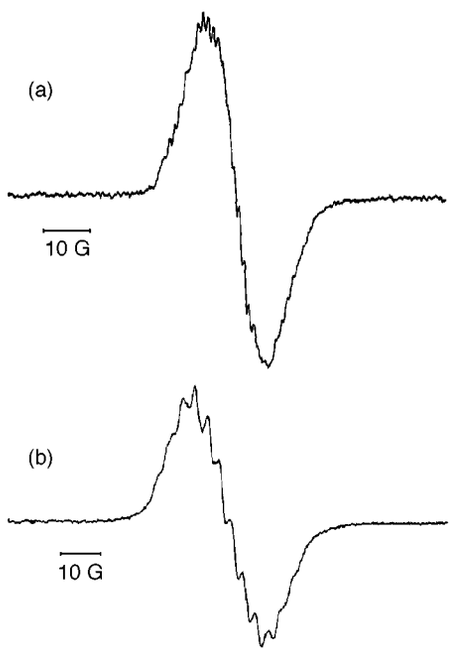

Fig. 5 The EPR spectra of **1b** (a) and **2b** (b) in THF at 298 K

free-electron value), are not well resolved, showing some hyperfine structure which probably originates from splitting due to the ^{14}N ($I = 1$, 99.63% abundance) and ^{1}H ($I = \frac{1}{2}$, 99.98% abundance) nuclei of the α-diimine ligand. Additional splitting, partly responsible for the poorly resolved EPR signals, may arise from the ^{99}Ru ($I = \frac{5}{2}$, 12.7% abundance) and ^{101}Ru ($I = \frac{5}{2}$, 17.1% abundance) nuclei, and from the ^{1}H nuclei bridging the cluster edges.

Elimination of H_2 from $[Ru_4(\mu\text{-}H)_4(CO)_{10}(L)]^{\cdot -/2-}$. Subsequent chemically irreversible one-electron reduction of the radical anions **1b** and **2b** at the cathodic potential $E(R_2)$ [see Table 4 and Fig. 3(A)] yielded **1c** and **2c**, respectively (see Tables 5 and 6). These compounds are identical with the species produced from **1b** and **2b** in a thermal, probably disproportionation[3] reaction (see above). The dianionic clusters **1c** and **2c** are also formed *via* the direct two-electron route, from unstable dianions $[Ru_4(\mu\text{-}H)_4(CO)_{10}(L)]^{2-}$ (L = bpym or dpp) produced during the one-electron reduction of **1b** and **2b**. The nature of the products **1c** and **2c** was elucidated by performing a (spectro)electrochemical study of the cluster **3**.

The reduction of **3** at $E(R_1)$ is shifted more negatively compared to the reduction potentials of **1** and **2** [see Fig. 3(B) and Table 4], being only partly chemically reversible at $\nu = 0.1$ V s^{-1} ($I_{pa}/I_{pc} \approx 0.5$). This result agrees with a predominantly bpy-localized one-electron cathodic step producing the unstable radical anion $[Ru_4(\mu\text{-}H)_4(CO)_{10}(bpy)]^{\cdot -}$ **3b**. Obviously, the more basic bpy ligand with a higher-lying π* LUMO in comparison with the bpym and dpp ligands is less suited to accommodate the added electron in this case. The radical anion **3b**, though still detectable on the reverse anodic scan due to its oxidation at $E(O_1)$ [see Fig. 3(B)], decomposes more rapidly than **1b** and **2b** and was not observed by IR, UV/VIS and EPR spectroscopy during spectroelectrochemical experiments at room temperature. Instead, the reduction of **3** on the time-scale of minutes yielded exclusively the dianion **3c**, as was judged from the close similarity of IR spectra of **1c**–**3c** (see Fig. 6, left, and Table 5). The UV/VIS spectrum of **3c** is depicted in Fig. 6, right.

The ν(CO) bands between 1800 and 1670 cm^{-1} in the IR spectra of **1c**–**3c** are indicative of bridging CO ligands which may have replaced some of the edge-bridging hydrogen atoms on the reduction of **1b**–**3b**. This behaviour is analogous to that reported for unsubstituted $[Ru_4(\mu\text{-}H)_4(CO)_{12}]$ whose irreversible two-electron reduction produces the dianion $[Ru_4(\mu\text{-}H)_2(CO)_{12}]^{2-}$ with three CO ligands bridging the basal Ru–Ru bonds.[3,22] We could obtain the latter species neatly *via* stepwise deprotonation of $[Ru_4(\mu\text{-}H)_4(CO)_{12}]$ in THF on addition of 2 equivalents of NEt_4OH in MeOH, in conformity with the

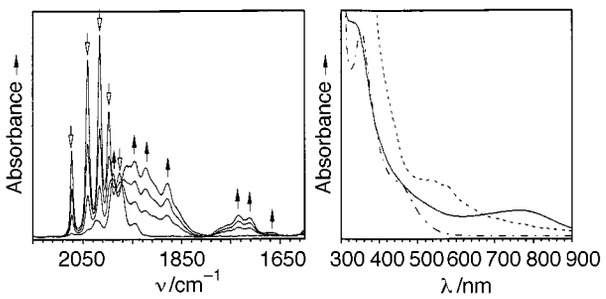

Fig. 6 Left: infrared spectral changes [ν(CO) region] accompanying the irreversible reduction of the cluster **3** producing the dianion **3c**. Right: UV/VIS spectra of **3** (dot-dash line), **3c** (full line) and the tetraanion **3e**, the 2e reduction product of **3c** (broken line). All spectra were recorded in THF at $T = 298$ K

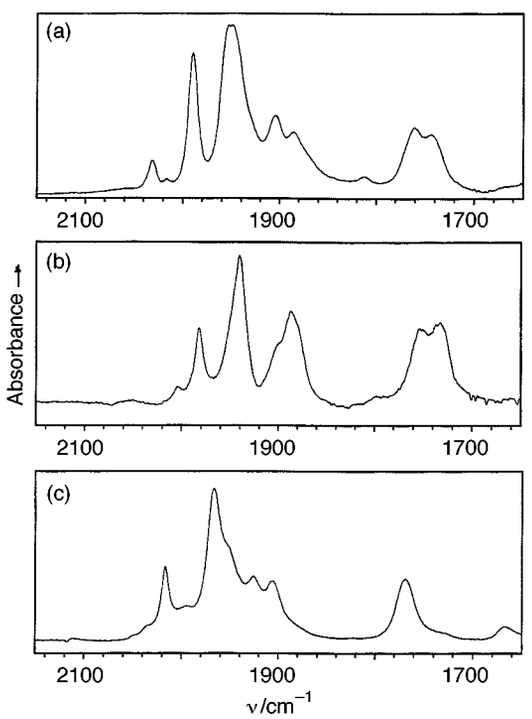

Fig. 7 The IR spectra [ν(CO) region] of (a) $[NEt_4]_2[Ru_4(\mu\text{-}H)_2(CO)_{12}]$, (b) **3c′** in MeCN, and (c) **3d** in MeCN. All spectra recorded at $T = 298$ K

recorded IR spectra attributed to the intermediate $NEt_4[Ru_4(\mu\text{-}H)_3(CO)_{12}]$ [ν(CO) at 2074w, 2038s, 2032 (sh), 2015s, 1990s cm^{-1}][23] and the yellow-orange final product $[NEt_4]_2[Ru_4(\mu\text{-}H)_2(CO)_{12}]$ [ν(CO) at 2031w, 1990s, 1951vs (br), 1904m, 1886m, 1814vw, 1761m, 1744m cm^{-1}][22] (see Fig. 7). The salt NEt_4OH was therefore chosen as a suitable reagent for the anticipated deprotonation of **3**. The reaction was performed in MeCN owing to poor solubility of the product(s) in THF. Initially a brown species **3c′** was formed whose IR spectrum closely resembled that of $[NEt_4]_2[Ru_4(\mu\text{-}H)_2(CO)_{12}]$ under the same conditions: ν(CO) at 2004w, 1982m, 1941vs, 1900 (sh), 1887m, 1797vw, 1754m, 1737m cm^{-1} (see Fig. 7). The smaller wavenumbers of **3c′** relative to those of $[NEt_4]_2[Ru_4(\mu\text{-}H)_2(CO)_{12}]$ (by *ca.* 10 cm^{-1}) point to co-ordination of the σ-donor 2,2′-bipyridine ligand, which was also evident from the ^1H NMR spectrum of **3c′** in CD_3CN. The signals of the bpy-protons of the parent cluster **3** [δ 9.01 (d, 2 H), 8.44 (d, 2 H), 8.20 (dt, 2 H), 7.64 (dt, 2 H)] were replaced after addition of NEt_4OH by a new set for **3c′** at δ 8.80 (d, 2 H), 8.26 (d, 2 H), 8.07 (t, 2 H) and 7.56 (t, 2 H). These values deviate from those for the uncoordinated 2,2′-bipyridine under identical conditions [δ 8.80 (d), 8.52 (d), 7.99 (dt) and 7.50 (dt)]. Notably, the cluster **3c′** could only be detected as an unstable intermediate. It transformed within a few minutes into another CO-bridged compound **3d** characterized by ν(CO) bands at 2034 (sh), 2017m, 1992 (sh), 1967vs, 1955 (sh), 1926m, 1907m, 1821vw, 1770m cm^{-1} (see Fig. 7) and, in the ^1H NMR spectrum, by resonances due to the bpy ligand at δ 8.68 (d, 2 H), 8.30 (d, 2 H), 8.09 (dt, 2 H), 7.56 (dt, 2 H) and broad hydride resonances at −16.8 (s, 1 H) and −23.7 (s, 1 H). Recall that the ^1H NMR spectrum of $[Ru_4(\mu\text{-}H)_2(CO)_{12}]^{2-}$ exhibits at room temperature only a sharp hydride singlet at δ −19.26.[22] Importantly, IR spectroelectrochemical experiments revealed that **3d** is identical to the product of electrochemical oxidation of **3c** at the anodic potential $E(O_2')$ (see Fig. 3 and Table 4). The nature of the conversion of **3c′** into **3d**, apparently demanding an oxidation step, was not investigated in detail. All attempts to crystallize **3d** have been unsuccessful so far.

In essence, the above IR and ^1H NMR data show that deprotonation of **3** yields **3c′** which can be formulated as the tetrahedral dianion $[Ru_4(\mu\text{-}H)_2(CO)_{10}(bpy)]^{2-}$, probably with three bridging CO ligands such as those established for the unsubstituted derivative $[Ru_4(\mu\text{-}H)_2(CO)_{12}]^{2-}$.[22] Successive electrochemical reduction of **3** and the radical anion **3b** ultimately yields **3c** exhibiting slightly lower ν(CO) wavenumbers and a different, more complex ν(CO) pattern with regard to those of **3c′** (see Figs. 6 and 7). The question remains how much **3c** corresponds to **3c′**. According to the IR spectra, these species are not identical. There is also no evidence that **3c** and **3c′** interconvert. The actual difference between them, however, is believed not to be significant as both identically produce **3d** (see above). For comparison, both electrochemical reduction[3] and deprotonation[22] of $[Ru_4(\mu\text{-}H)_4(CO)_{12}]$ yielded the same product, *viz.* $[Ru_4(\mu\text{-}H)_2(CO)_{12}]^{2-}$. At this stage of investigation we can conclude that, similarly to **3c′**, the electrochemical reduction product **3c** is also a dianionic Ru_4-cluster with edge-bridging hydride and carbonyl ligands, formed from the transient cluster $[Ru_4(\mu\text{-}H)_4(CO)_{10}(bpy)]^{2-}$ *via* elimination of H_2.

The very similar averaged ν(CO) wavenumbers and the almost α-diimine-independent oxidation potentials $E(O_2')$ of the dianions **1c**–**3c** (see Tables 4 and 5) imply effective delocalization of the negative charge over the cluster core, residing more at the CO-bridged basal $Ru_3(CO)_9$ moiety than at the apical Ru(α-diimine) fragment. The UV/VIS spectrum of **3c** exhibits a broad band at 763 nm which may belong to Ru(bpy)-localized electronic transitions, for $[Ru_4(\mu\text{-}H)_2(CO)_{12}]^{2-}$ does not absorb at such a low energy.

Further reduction of **3c** at the electrode potential $E(R_3)$, studied by IR/UV/VIS spectroelectrochemistry, yielded the cluster **3e** (see Table 5). The CO-bridge absorptions in the IR spectrum of **3c** shifted on the reduction to lower wavenumbers by approximately 30 cm^{-1}, which is slightly more than that found for $[N(PPh_3)_2]_2[Ru_4(\mu\text{-}H)_2(CO)_{12}]$[22] and $[Ph_4P]_4[Ru_4(CO)_{12}]$.[24] The UV/VIS spectrum of **3e** shows a broad structured band with maxima at 533 and 572 nm and shoulders at 505, 640, 700 and 760 nm (see Fig. 6). These features strongly resemble the visible absorption of the two-electron-reduced anion $[Re(CO)_3(bpy)]^-$ having the added two electrons strongly π-delocalized over the Re(bpy) chelate ring.[25,26] We may thus assign **3e** as $[NBu_4]_4[Ru_4(CO)_{10}(bpy)]$, with the two extra electrons added to the dianion **3c** predominantly residing on the π-system of the Ru(bpy) moiety. According to the cyclic voltammograms of **2** and **3**, the reduction of **3c** at $E(R_3)$ should be a one-electron process which affords the radical $[\mathbf{3c}]^{\bullet -}$. This transient species was indeed observed in the course of the UV/VIS OTTLE experiment. Its UV/VIS spectrum exhibits a characteristic structured band with absorption maxima at 495 and 522 nm, belonging to an intraligand electronic transition of the one-electron-reduced ligand $[bpy]^{\bullet -}$.[27] The radical $[\mathbf{3c}]^{\bullet -}$ probably further disproportionated into **3c** and **3e** under liberation of H_2. Recall that reduction of $[Ru_4(\mu\text{-}H)_2(CO)_{12}]^{2-}$ is also initially a one-electron process;[3] although, deprotonation of the dianion with 1 equivalent of KH only produced a 1:1 mixture of $[Ru_4(\mu\text{-}H)_2(CO)_{12}]^{2-}$ and $[Ru_4(CO)_{12}]^{4-}$.[22] In fact, the

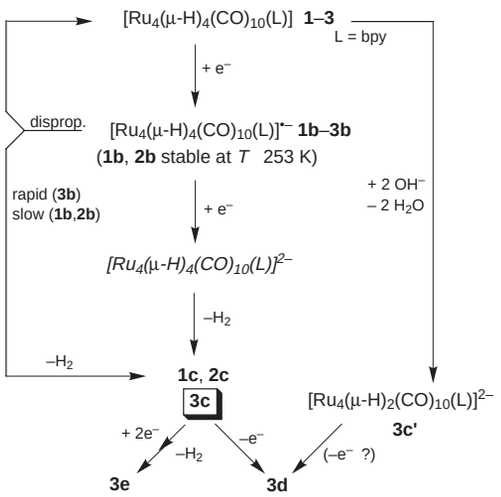

Scheme 2 Reduction paths of the clusters $[Ru_4(\mu\text{-}H)_4(CO)_{10}(L)]$

only reported route to $[Ru_4(\mu\text{-}H)(CO)_{12}]^{3-}$ involved protonation of $[Ru_4(CO)_{12}]^{4-}$ with HBr.[24] The reduction path of **1**–**3** is summarized in Scheme 2.

Oxidation of $[Ru_4(\mu\text{-}H)_4(CO)_{10}(L)]$ 10. The cyclic voltammograms of **2** and **3** in Fig. 3 reveal that these clusters undergo chemically irreversible oxidation consuming more than one electron $[I_a(O_m) \approx 2I_c(R_1)]$. The very close values of the corresponding anodic peak potentials $E(O_m)$ (see Table 4) are indicative of an anodic process localized on the metal core, which may induce cleavage of Ru–Ru bonds. The oxidation of $[Ru_4(\mu\text{-}H)_4(CO)_{10}(L)]$ was not further investigated.

Comparison of the reduction paths of $[Ru_4(\mu\text{-}H)_4(CO)_{10}(L)]$ and $[Os_3(CO)_{10}(L)]$. Both $[Ru_4(\mu\text{-}H)_4(CO)_{10}(L)]$ and $[Os_3(CO)_{10}(L)]$[4] (L = bpym, dpp or bpy) initially undergo one-electron reduction mainly localized on the lowest π* orbital of the α-diimine ligand. The corresponding radical anionic products are therefore substantially more stable than those derived from the unsubstituted clusters $[Ru_4(\mu\text{-}H)_4(CO)_{12}]$[3] and $[Os_3(CO)_{12}]$,[28] and can be detected by diverse spectroelectrochemical methods. The reactivity induced by reduction of these low-nuclearity clusters can conveniently be controlled by tuning the electronic properties of the α-diimine ligands L. Raising the σ,π-donor character of the reduced α-diimine initiates secondary chemical/electron transfer reactions of the radical anions, whose nature is identical with the reactivity of the purely carbonyl precursors. In particular, the species $[Os_3(CO)_{12-2n}(L)_n]^{\bullet-}$ ($n = 0$ or 1) undergo cleavage of an Os–Os bond resulting ultimately in formation of open-structure dianionic clusters.[4] Contrary to this, the species $[Ru_4(\mu\text{-}H)_4(CO)_{12-2n}(L)_n]^{\bullet-}$ ($n = 0$ or 1) react *via* the loss of hydrogen to give the corresponding dianions $[Ru_4(\mu\text{-}H)_2(CO)_{12-n}(L)_n]^{2-}$. Notably, we have obtained no spectroscopic evidence for participation of the anion $[Ru_4(\mu\text{-}H)_3(CO)_{10}(L)]^-$ in the reduction path of $[Ru_4(\mu\text{-}H)_4(CO)_{10}(L)]$, as was reported[3] for the reduction of $[Ru_4(\mu\text{-}H)_4(CO)_{12}]$.

The radical anions $[Ru_4(\mu\text{-}H)_4(CO)_{10}(L)]^{\bullet-}$ are apparently more stable than the corresponding species $[Os_3(CO)_{10}(L)]^{\bullet-}$. In the latter case only $[Os_3(CO)_{10}(bpym)]^{\bullet-}$ could be characterized spectroscopically, becoming stable at $T = 213$ K. The radical $[Os_3(CO)_{10}(dpp)]^{\bullet-}$ is only stable on a subsecond time-scale of cyclic voltammetry while $[Os_3(CO)_{10}(bpy)]^{\bullet-}$ partly decomposes at moderate scan rates even at $T = 220$ K and at room temperature it is not detectable at all.[4] The order of increasing stability of the radical anions on co-ordination of stronger π-acceptor L, bpy ≪ dpp < bpym, applies also for $[Ru_4(\mu\text{-}H)_4(CO)_{10}(L)]^{\bullet-}$. All the latter species could be detected by conventional cyclic voltammetry at room temperature and, for L = dpp or bpym, they were also characterized by IR, UV/VIS and EPR spectroscopy. The large difference in the stability of $[Ru_4(\mu\text{-}H)_4(CO)_{10}(L)]^{\bullet-}$ and the corresponding Os_3 derivatives can be ascribed to a more delocalised bonding situation in the robust closely-packed tetrahedral $Ru_4(\mu\text{-}H)_4$ core.

Conclusion

The co-ordination of the reducible α-diimine ligand L in the novel clusters $[Ru_4(\mu\text{-}H)_4(CO)_{10}(L)]$ prevents rapid decomposition of the primary one-electron reduction products. The radical anions $[Ru_4(\mu\text{-}H)_4(CO)_{10}(L)]^{\bullet-}$ (L = dpp or bpym) are stable on the time-scale of minutes and could be characterized by IR, UV/VIS and EPR spectroscopy. Regardless of this stabilizing influence, the overall reactivity remains unaffected. Either on uptake of another electron, or thermally *via* disproportionation, the radical anions $[Ru_4(\mu\text{-}H)_4(CO)_{10}(L)]^{\bullet-}$ lose dihydrogen and transform to dianions $[Ru_4(\mu\text{-}H)_2(CO)_{10}(L)]^{2-}$ which contain edge-bridging CO ligands. The reactivity is highest for $[Ru_4(\mu\text{-}H)_4(CO)_{10}(bpy)]^{\bullet-}$ which could only be observed by cyclic voltammetry. In this respect, the reactivity of $[Ru_4(\mu\text{-}H)_4(CO)_{10}(L)]^{\bullet-}$ parallels that of unsubstituted $[Ru_4(\mu\text{-}H)_4(CO)_{12}]^{\bullet-}$.

Acknowledgements

We thank the Netherlands Foundation of Chemical Research (SON), the Netherlands Organization for Scientific Research (NWO) and the University of Edinburgh for financial assistance. Professor L. J. Yellowlees, Dr. N. Payne, Dr. S. Parsons and Dr. A. J. Blake (all from the University of Edinburgh) are jointly acknowledged for their helpful contributions to this work.

References

1 L. N. Lewis, *Chem. Rev.*, 1993, **93**, 2693.
2 Y. Doi, S. Tamura and K. Koshizuka, *J. Mol. Cat.*, 1983, **19**, 213; *Inorg. Chim. Acta*, 1982, **65**, L63.
3 D. Osella, C. Nervi, M. Ravera, J. Fiedler and V. V. Strelets, *Organometallics*, 1995, **14**, 2501.
4 F. Hartl, J. W. M. van Outersterp and D. J. Stufkens, *Organometallics*, submitted for publication; J. W. M. van Outersterp, Ph.D. Thesis, University of Amsterdam, 1995.
5 F. Piacenti, M. Bianchi, P. Frediani and E. Benedetti, *Inorg. Chem.*, 1971, **10**, 2759.
6 M. Bianchi, P. Frediani, A. Salvini, L. Rosi, L. Pistolesi, F. Piacenti, S. Ianelli and M. Nardelli, *Organometallics*, 1997, **16**, 482.
7 S. A. R. Knox, J. W. Koepke, M. A. Andrews and H. D. Kaesz, *J. Am. Chem. Soc.*, 1975, **97**, 3942.
8 G. M. Sheldrick, SHELXS 86, Program for the Solution of Crystal Structures, *Acta Crystallogr., Sect. A*, 1990, **46**, 467; SHELXL 93, University of Göttingen, 1993; C. K. Johnson, ORTEP, Report ORNL-5138, Oak Ridge National Laboratory, Oak Ridge, TN, 1976.
9 G. Gritzner and J. Kuta, *Pure Appl. Chem.*, 1984, **56**, 461.
10 M. Krejčík, M. Daněk and F. Hartl, *J. Electroanal. Chem. Interfacial Electrochem.*, 1991, **317**, 179.
11 F. Hartl, H. Luyten, H. A. Nieuwenhuis and G. C. Schoemaker, *Appl. Spectrosc.*, 1994, **48**, 1522.
12 R. R. Andréa, H. Luyten, M. A. Vuurman, D. J. Stufkens and A. Oskam, *Appl. Spectrosc.*, 1986, **40**, 1184.
13 J. W. M. van Outersterp, M. T. Garriga Oostenbrink, H. A. Nieuwenhuis, D. J. Stufkens and F. Hartl, *Inorg. Chem.*, 1995, **34**, 6312.
14 G. Freeman, L. J. Yellowlees, S. I. Ingham and B. F. G. Johnson, unpublished work.
15 S. A. R. Knox and H. D. Kaesz, *J. Am. Chem. Soc.*, 1971, **93**, 4594.
16 M. J. Schadt, M. Gresalfi and A. J. Lees, *Inorg. Chem.*, 1985, **24**, 2942.
17 A. U. Härkönen, M. Ahlgrén, T. A. Pakkanen and J. Pursiainen, *J. Organomet. Chem.*, 1997, **530**, 191.
18 J. W. M. van Outersterp, F. Hartl and D. J. Stufkens, *Organometallics*, 1995, **14**, 3303.
19 W. Kaim, S. Kohlmann, A. J. Lees, T. L. Snoeck, D. J. Stufkens and M. M. Zulu, *Inorg. Chim. Acta*, 1993, **210**, 159.

20 R. Greef, R. Peat, L. M. Peter, D. Pletcher and J. Robinson, in *Instrumental Methods in Electrochemistry*, ed. T. J. Kemp, Ellis Horwood, Chichester, 1985, ch. 6, p. 186.
21 P. S. Braterman, J.-I. Song, C. Vogler and W. Kaim, *Inorg. Chem.*, 1992, **31**, 222.
22 K. E. Inkrott and S. G. Shore, *Inorg. Chem.*, 1979, **18**, 2817.
23 J. W. Koepke, J. R. Johnson, S. A. R. Knox and H. D. Kaesz, *J. Am. Chem. Soc.*, 1975, **97**, 3947.
24 A. A. Bhattacharyya, C. C. Nagel and S. G. Shore, *Organometallics*, 1983, **2**, 1187.
25 G. J. Stor, F. Hartl, J. W. M. van Outersterp and D. J. Stufkens, *Organometallics*, 1995, **14**, 1115.
26 B. D. Rossenaar, F. Hartl and D. J. Stufkens, *Inorg. Chem.*, 1996, **35**, 6194.
27 M. Krejčík and A. A. Vlček, *J. Electroanal. Chem. Interfacial Electrochem.*, 1991, **313**, 243.
28 A. J. Downard, B. H. Robinson, J. Simpson and A. M. Bond, *J. Organomet. Chem.*, 1987, **320**, 363.

Received 16*th April* 1998; *Paper* 8/02849D